SUPPLEMENTARY MATERIALS TO

Deazaflavin cofactor boosts earthworms *Henlea* bioluminescence

8-hydroxy-10-(2,3,4,5-tetrahydroxypentyl)pyrimido[4,5-b]-quinoline-2,4(3H, 10H)dion (4):
25

Materials and methods

Chemicals, unless otherwise stated, were obtained from Sigma-Aldrich (St. Louis, MO, USA) at the purest grade available. Merck Kieselgel 60 was used for column chromatography. Thin layer chromatography was performed on silica gel 60 F254 aluminium-backed plates (Merck), solvent systems: $CHCl_3$/EtOH. Visualization was effected by UV light (254 or 365 nm) and staining with $KMnO_4$ solutions.

Extraction and purification procedures

Extraction of low-molecular-weight compounds from biomass

The activators were isolated as by-products during the multi-stage chromatographic purification of *Henlea sp.* luciferin. The procedure was described in detail in the article (Petushkov and Rodionova 2018) and then slightly modified. *Henlea sp.* collected from soil were washed and frozen in 100-specimen portions for further experiments. A two portions of frozen biomass (200 specimens) was homogenized in 12 mL water/methanol (1:2) at 0°C and the obtained homogenate centrifuged (16000g, 20 min) to remove the majority of the high-molecular-weight compounds; The supernatant (13 ml total) containing luciferin was brightly fluorescent under UV irradiation. Subsequent evaporation (Vac-Rotor Concentrator Type 350P, Unipan Scientific Instruments, Warsaw, Poland) yielded 1 ml of concentrated low-molecular-weight fraction.

Chromatographic purification of the luciferin and activators

To concentrate and separate the luciferin-containing fraction by solid-phase extraction, the concentrated supernatant was acidified by the addition of conc. HCl (10 µl) and loaded onto a disposable 1mL C16 extraction cartridge (Diapack- C16, BioChemMak S&T, Moscow, Russia). After washing the column with 0.5 mL 30mM HCl, the target fraction was eluted with 3 mL methanol and adjusted to a minimum volume of 200 µL on a rotary evaporator. Then, luciferin-containing fraction was subjected to a multistage purification by HPLC in an Agilent 1260 Infinity chromatograph (Agilent Technology, United States) equipped with a DAD detector on different columns (Agilent Technology): reverse-phase ZORBAX Eclipse XDB-C18 column (4.6 × 250 mm) in a gradient of acetonitrile (ACN) in 0.1% formic acid (5-40%) for 20 minutes at a rate of 1 ml/min, temperature 35°C; ZORBAX Eclipse XDB-C18 column (3×150 mm) in a gradient of acetonitrile in 0.1% formic acid (1–40%) for 10 min at a rate of 1 mL/min; and anion exchange ZORBAX SAX column (4.6×150 mm) with the elution

of the target fractions with 0.1 M KH$_2$PO$_4$ solution (pH 4.6) at a rate of 1 mL/min. The final gel-filtration purification was performed on a SuperdexPeptide 10/300 GL column (GE HealthCare Life Sciences, United States) with elution of fractions with 50 mM ammonium formate (pH 4.6) at a rate of 0.8 mL/min.

During the chromatographic purification of luciferin we detected an unduly drastic decrease of its total activity. We assumed this was because of the loss of a certain component required for the luminescent reaction. To find that hypothetical substance we tracked the distribution of other compounds and checked their influence on bioluminescence activity enhancement in cross-tests. Thus, at the first chromatographic stage (ZORBAX Eclipse XDB-C18 column (4.6 × 250 mm), we identified two peaks (retention times 10.16 minutes and 10.85 minutes) that caused a multifold increase of the bioluminescence of the reaction mixture. These fractions, called "Activator H" and "Activator S," (shortened ActH and ActS in this manuscript) were fractionated and then re-chromatographed on anion exchange ZORBAX SAX column and SuperdexPeptide 10/300 GL column separately.

Purification of native luciferase

Purified samples of luciferase were obtained in a single-step purification procedure by gel filtration. Crude water extract of luciferase obtained through homogenization of a 100 specimens of frozen worms in water 4mL, maximum cell disruption and extraction was achieved through additional freezing and thawing of biomass, was subjected to centrifugation for 20 min at 14000g. 500 µL of supernatant was fractionated on a Superdex 200 10/300 GL column (GE HealthCare Life Sciences, United States) with the elution of fractions with 50 mM MOPS pH 7 (pH 4.6) at 0.5 mL/ min. A significant amount of activators was separated from proteins during chromatography, which could be traced by the characteristic UV absorption spectrum and fluorescence of low-molecular-weight fractions.

Luminescence measurement assey

Reactions were monitored with a custom made luminometer Oberon-K (Krasnoyarsk, Russia) at 20°C. For each measurement reaction mixtures consisting of 100 µl of 16 mM MOPS buffer, pH 7.0, containing 1 mM CaCl$_2$, 2 µl of pre-activated highly purified *Henlea sp.* luciferin and 2 µl of partially purified luciferase fraction (after gel filtration) were used. Measurements were corrected for background luminescence of luciferase based on monitoring reactions for 20 s prior to the addition of 2 µl of the synthetic ActH chromophore at various concentrations. Final concentrations of ActH were calculated from isosbestic point at 401 mn, using molar extinction coefficient 25.9 mM^{-1}cm^{-1} of structurally similar factor F$_{420}$ (DiMarco et al. 1990).

Multifold activation essay (Figure 7d)

Reaction mixture at start was prepared as follows: 100 µl of 16мM MOPS buffer with 1 mM of CaCl$_2$, 2 µl of native purified luciferase, 2 µl of synthetic ActH (10 o.d.u). Purified *Henlea* luciferin aliquots (2µl) were mixed with the same MOPS buffer with CaCl$_2$ (10µl) and pre-activated by heating to 95°C and subsequent cooling to 20°C. In samples I and II heating/cooling times was 60 seconds, for sample III heating/cooling time was reduced to 30 seconds. Only 10 µl out of 12 µl of the pre-activated luciferin was added to the reaction mixture.

Mass spectrometry

LCMS spectra were acquired using Thermo Orbitrap Elite hybrid instrument with Thermo Accela UPLC system equipped with Phenomenex Aeris XB-C8 widepore column (150 × 2.1 mm, 3.6 um). Samples were eluted with a H2O-MeCN gradient (from 5 to 55% of MeCN) with 0.1% formic and 0.02% trifluoroacetic acids as eluent additive.Detection was achieved by UV-VIS DAD, full scan MS (ESI+/-, 250-2000 au) and data-dependent MS2(CID activation, NCE 35%).

Flow infusion MSn analysis was performed on Thermo LTQ Orbitrap XL hybrid instrument. Samples were dissolved in 0.1% acetic acid and infused via syringe pump af flow rate 5 ul/min. Fragmentation energy was tuned manually at each fragmentation step to achieve maximum fragment ion intensity.

NMR spectroscopy

NMR spectra of purified activators ActH and ActS were acquired on Bruker Avance III 600 MHz NMR (ActH) and 800 MHz NMR (ActS) both equipped with cryogenically cooled probes. The samples were dissolved in D_2O and pH was adjusted by DCl aliquots to an acidic value because of a higher quality of the ^1H NMR spectra (data not shown). Finally, temperature was 10°C and pH was 2.6 for ActH and 3.5 for ActS in all the NMR experiments used for structure elucidation. Chemical shifts were referenced to the residual HOD signal expected at 4.942 ppm at 10°C (Gottlieb et al. 1997). Probable sample degradation was controlled by ^1H NMR at least once per day and no visible changes in the NMR were identified.

The low quantity of both ActH and ActS required a long term NMR data acquisition for more than a week for both of them. Namely, for ActH the ^1H NMR (Figure 3**b**) acquired for 37 minutes, 2D [^1H,^{13}C] HSQC (Figure 4**c-f**) took 21 hours with a low S/N = 5. Through-space 2D ROESY was acquired for 17.5 hours, 2D COSY (Figure 4**a,b**) for 8 hours, 2D [^1H,^{13}C] HMBC (Figure 4**e-f**) was acquired 5 (five) times 23 hours each spectrum (interleaved with 37 minutes ^1H), hence as much as 5 NMR days were spent for the HMBC accumulation. We did not observe any visible NMR cross-peaks in the individual five 2D [^1H,^{13}C] HMBC spectra; the structural information was observed and resolved only after addition of all five 2D NMR experiments. In the same way, 2D [^1H,^{13}C] HMBC of ActS was accumulated during 7 (seven) days, the structural cross-peaks were visible only after addition of all seven HMBC spectra.

Once the initial hypothesis about the ActH chemical structure was proposed, the NMR spectra of ActH were additionally re-acquired in d_4-MeOD for direct comparison with the literature data (Kuo et al. 1989). We again observed higher quality of the ^1H NMR spectra at acidic pH (in MeOD), the pH meter reading in MeOD was 4.9, temperature 10°C, the data acquired at 800 MHz. No 2D [^1H,^{13}C] HMBC was re-accumulated in MeOD, only ^1H and 2D [^1H,^{13}C] HSQC were used for structure dereplication. The NMR spectra of synthetic ActH (archaeal cofactor F0) were obtained at 700 MHz in d_4-MeOD at 10°C in acidic pH (the pH-meter reading was 3.3).

Raw data availability

The raw MS data of ActH and ActS from *Henlea sp.* deep fragmentation in positive and negative ionization modes is available on GoogleDrive by the following link:

https://drive.google.com/drive/folders/11mxcVzisKOtpU3qD6mptbxi8ZpMPnMJL?usp=sharing

The raw NMR data (FIDs and processed spectra) of ActH from *Henlea sp.* (D_2O and MeOD), synthetic ActH (MeOD), ActS from *Henlea sp.* (D_2O) and three intermediates of the ActH synthesis ($CDCl_3$) are available on GoogleDrive by the following link:

https://drive.google.com/drive/folders/1OyvpBP_5MUsMxT1pfRQlqForgMUuTNmd?usp=sharing

MSn data of ActH and ActS

Table S1. Ambiguities in the interpretation of the MSn data of ActH in negative ionization mode

Ambiguities in the interpretation of the MSn data of ActH in negative ionization mode. The observed masses are bold in gray rectangles. The 362 parent ion has five self-consistent brutto formula interpretations. They are highlighted with different colors, corresponding brutto formulae of three neutral losses together with three daughter ions are highlighted with the same colors. Deviations from theoretical masses by more than 5 ppm are highlighted with red bold frames. The brutto formula $C_{16}H_{17}N_3O_7$ highlighted with yellow color was finally accepted. RDB - Ring and Double Bond equivalents.

Full MS	Theory	delta, mDa	delta ppm	RDB	Neutral loss	Theory	delta, mDa	delta, ppm	RDB	MS2	Theory	delta, mDa	delta, ppm	RDB
362.09832					**18.01073**					**344.08759**				
$C_{16}H_{17}N_3O_7$	362.09938	1.056	2.916	10	H_2O	18.01057	-0.165	-9.161	0	$C_{16}H_{15}N_3O_6$	344.08881	1.221	3.549	11
$C_{12}H_{13}N_9O_5$	362.09669	-1.630	-4.502	11						$C_{12}H_{11}N_9O_4$	344.08613	-1.465	-4.258	12
$C_{17}H_{13}N_7O_3$	362.10071	2.392	6.606	15						$C_{17}H_{11}N_7O_2$	344.09015	2.557	7.431	16
$C_{11}H_{17}N_5O_9$	362.09535	-2.966	-8.191	6						$C_{11}H_{15}N_5O_8$	344.08479	-2.801	-8.140	7
$C_5H_{17}N_9O_{10}$	362.10257	4.245	11.723	2						$C_5H_{15}N_9O_9$	344.09200	4.410	12.817	3
					120.04205					**242.05627**				
					$C_4H_8O_4$	120.04226	0.210	1.749	1	$C_{12}H_9N_3O_3$	242.05712	0.846	3.495	10
					$C_4H_8O_4$	120.04226	0.210	1.749	1	$C_8H_5N_9O$	242.05443	-1.840	-7.602	11
					$C_5H_4N_4$	120.04360	1.546	12.879	6	$C_{12}H_9N_3O_3$	242.05712	0.846	3.495	10
					$C_4H_8O_4$	120.04226	0.210	1.749	1	$C_7H_9N_5O_5$	242.05309	-3.176	-13.121	6
					$C_4H_8O_4$	120.04226	0.210	1.749	1	$CH_9N_9O_6$	242.06031	4.035	16.670	2
					134.05758					**228.04074**				
					$C_5H_{10}O_4$	134.05791	0.330	2.462	1	$C_{11}H_7N_3O_3$	228.04147	0.726	3.184	10
					$C_5H_{10}O_4$	134.05791	0.330	2.462	1	$C_7H_3N_9O$	228.03878	-1.960	-8.595	11
					$C_6H_6N_4$	134.05925	1.666	12.427	6	$C_{11}H_7N_3O_3$	228.04147	0.726	3.184	10
					$C_5H_{10}O_4$	134.05791	0.330	2.462	1	$C_6H_7N_5O_5$	228.03744	-3.296	-14.454	6
					$C_5H_{10}O_4$	134.05791	0.330	2.462	1	$H_7N_9O_6$	228.04466	3.915	17.168	2

Table S2. Ambiguities in the interpretation of the MSn data of ActS in negative ionization mode

Ambiguities in the interpretation of the MSn data of ActS MS2 362 ion in negative ionization mode. All the notations are the same as in the previous table.

MS2	Theory	delta, mDa	delta, ppm	RDB	Neutral loss	Theory	delta, mDa	delta, ppm	RDB	MS3	Theory	delta, mDa	delta, ppm	RDB
362.10031					**18.01083**					**344.08948**				
$C_{17}H_{13}N_7O_3$	362.10071	0.402	1.110	15	H_2O	18.01057	-0.265	-14.713	0	$C_{17}H_{11}N_7O_2$	344.09015	0.667	1.938	16
$C_{16}H_{17}N_3O_7$	362.09938	-0.934	-2.579	10						$C_{16}H_{15}N_3O_6$	344.08881	-0.669	-1.944	11
$C_5H_{17}N_9O_{10}$	362.10257	2.255	6.228	2						$C_5H_{15}N_9O_9$	344.09200	2.520	7.324	3
$C_{28}H_{13}N$	362.09752	-2.787	-7.697	23						**No solution**				
$C_{21}H_{17}NO_5$	362.10340	3.088	8.528	14						$C_{21}H_{15}NO_4$	344.09283	3.353	9.745	15
$C_{12}H_{13}N_9O_5$	362.09669	-3.620	-9.997	11						$C_{12}H_{11}N_9O_4$	344.08613	-3.355	-9.750	12
$C_{22}H_{13}N_5O$	362.10473	4.424	12.218	19						$C_{22}H_{11}N_5$	344.09417	4.689	13.627	20
					120.04270					**242.05761**				
					$C_5H_4N_4$	120.04360	0.896	7.464	6	$C_{12}H_9N_3O_3$	242.05712	-0.494	-2.041	10
					$C_4H_8O_4$	120.04226	-0.440	-3.665	1	$C_{12}H_9N_3O_3$	242.05712	-0.494	-2.041	10
					$C_4H_8O_4$	120.04226	-0.440	-3.665	1	$CH_9N_9O_6$	242.06031	2.695	11.134	2
					$C_4H_8O_4$	120.04226	-0.440	-3.665	1	$C_{17}H_9NO$	242.06114	3.528	14.575	14
					$C_4H_8O_4$	120.04226	-0.440	-3.665	1	$C_8H_5N_9O$	242.05443	-3.180	-13.137	11
					$C_5H_4N_4$	120.04360	0.896	7.464	6	$C_{17}H_9NO$	242.06114	3.528	14.575	14
					134.05831					**228.04200**				
					$C_6H_6N_4$	134.05925	0.936	6.982	6	$C_{11}H_7N_3O_3$	228.04147	-0.534	-2.342	10
					$C_5H_{10}O_4$	134.05791	-0.400	-2.984	1	$C_{11}H_7N_3O_3$	228.04147	-0.534	-2.342	10
					$C_5H_{10}O_4$	134.05791	-0.400	-2.984	1	$H_7N_9O_6$	228.04466	2.655	11.643	2
					$C_5H_{10}O_4$	134.05791	-0.400	-2.984	1	$C_{16}H_7NO$	228.04549	3.488	15.295	14
					$C_5H_{10}O_4$	134.05791	-0.400	-2.984	1	$C_7H_3N_9O$	228.03878	-3.220	-14.120	2
					$C_6H_6N_4$	134.05925	0.936	6.982	6	$C_{16}H_7NO$	228.04549	3.488	15.295	14

Figure S1. MSn fragmentation tree of ActH in positive ionization mode

Figure S1. **Complete MSn fragmentation tree of ActH in positive ionization mode**. Red numbers are observed m/z ions, red arrows show CID (collision induced dissociation) of observed ions, black brutto formulae are proposed interpretations of each m/z ion and corresponding neutral losses. Long fragmentation path highlighted with yellow picks the most represented daughter ion at each fragmentation step, this path was used to resurrect an actual brutto formula of ActH. All brutto forumae M are in neutral form assuming that observed positive ions are [M+H]+. See also figure 2 in the main text for the raw mass spectra of FullMS and MS2.

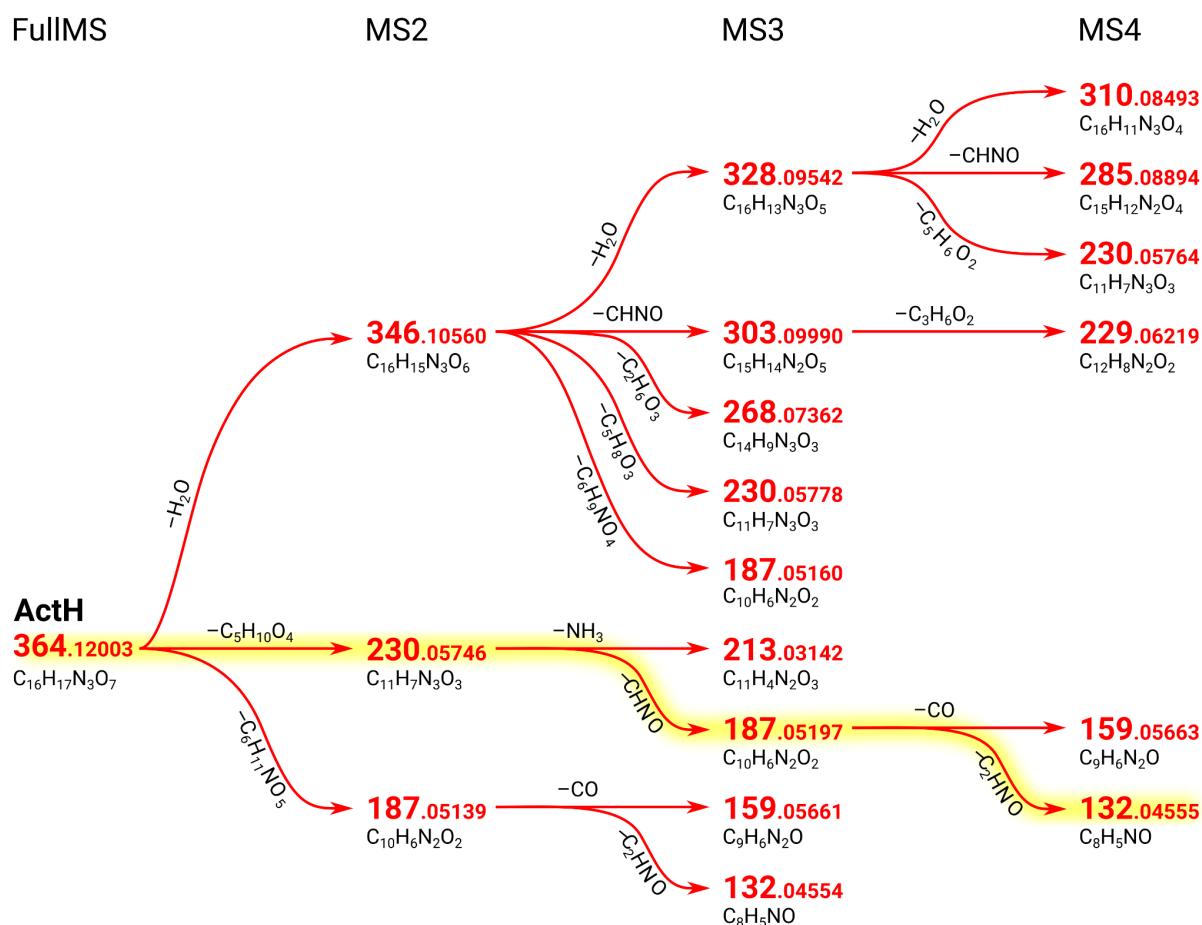## Figure S2. MSn fragmentation tree of ActH in negative ionization mode

Figure S2. **Complete MSn fragmentation tree of ActH in negative ionization mode**. Blue numbers are observed m/z ions, blue arrows show CID (collision induced dissociation) of observed ions, black brutto formulae are proposed interpretations of each m/z ion and corresponding neutral losses. All brutto forumae M are in neutral form assuming that observed negative ions are [M–H]$^-$. See also figure 2 in the main text for the raw mass spectra of FullMS, MS2 and MS3.

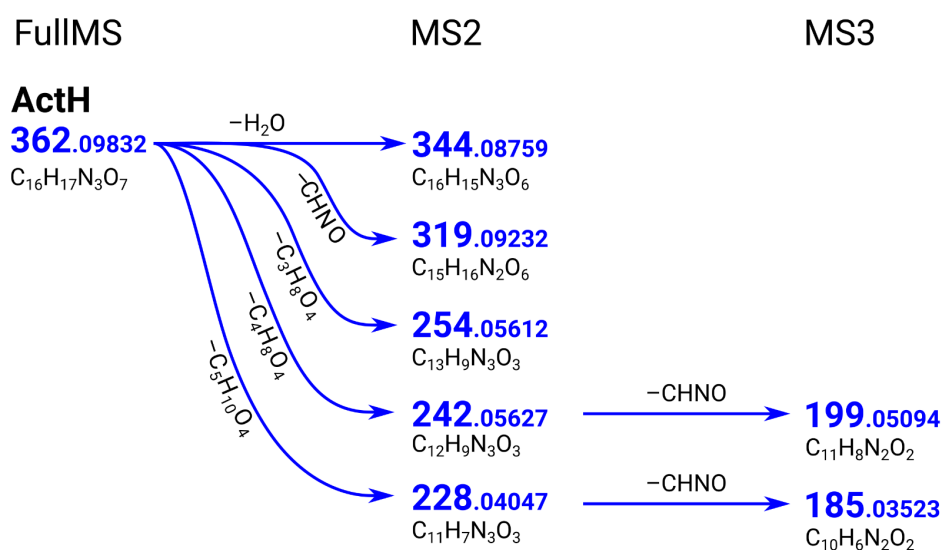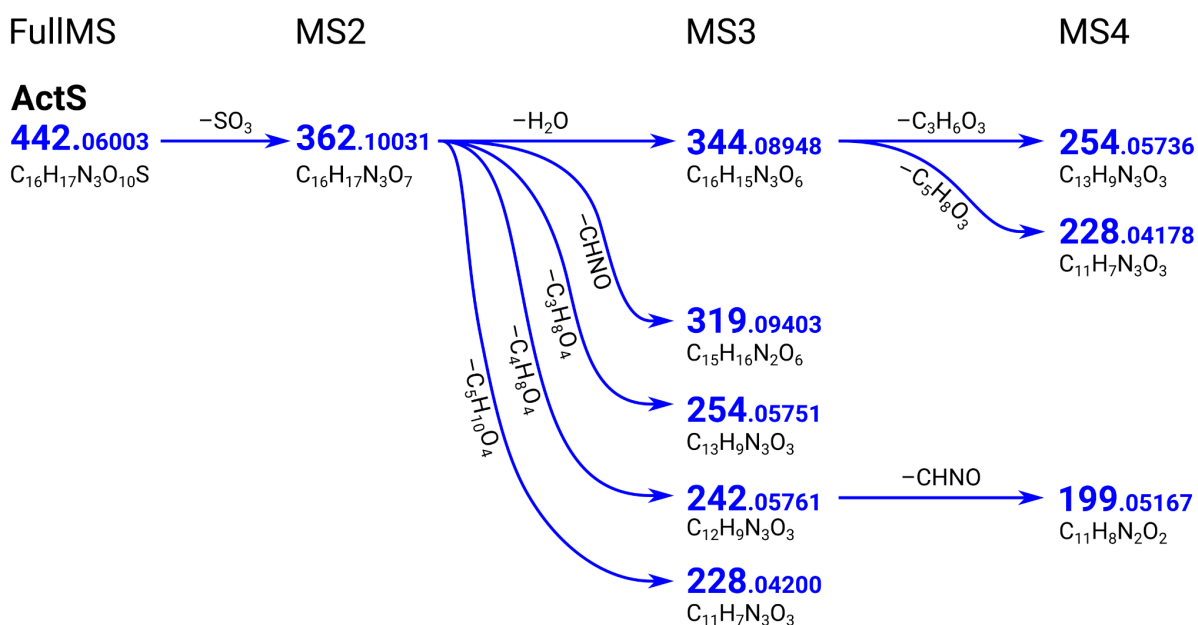## Figure S3. MSn fragmentation tree of ActS in negative ionization mode

Figure S3. **Complete MSn fragmentation tree of ActS in negative ionization mode**. All notations are the same as on the the previous figure S2

Chemical shifts of ActH and ActS

Table S4. Chemical shifts of ActH (600 MHz) in D$_2$O and MeOD

Chemical shifts of ActH at 600 MHz. ^{1}H and ^{13}C chemical shifts and ^{1}H multiplicities of observed NMR signals of ActH in D$_2$O and MeOD. For atom numbering see figure S4A below

#	ActH D$_2$O		^{13}C, ppm	ActH MeOD		^{13}C, ppm
	^{1}H, ppm and multiplicity			^{1}H, ppm and multiplicity		
5	9.032	s	143.78	8.964	s	142.29
5a			117.09			
6	8.039	d 8.7	134.47	7.995	d 8.7	133.70
7	7.208	dd 8.7;1.4	116.71	7.118	dd 8.7;1.4	116.20
9	7.446	d 1.4	101.60	7.540	d 1.4	101.79
9a			144.00			
10a			157.92			
2'	4.407	m	69.37	4.439	m	70.35
3'	3.902	dd 5.3;6.9	72.90	3.805	dd 5.3;6.9	73.92
4'	3.950	dt 2.4;6.8	71.96	3.891	dt 2.4;6.8	72.75
5'H2 5'H3	3.852 3.699	dd 2.4;11.7 dd 6.8;11.7	62.25	3.876 3.704	dd 2.3;11.5 dd 6.5;11.5	63.40

[a)] Observed as cross-peak in ^{13}C-HSQC from corresponding directly attached proton

[b)] Observed as cross-peak in ^{13}C-HMBC from the singlet proton 5 near 9 ppm

[c)] The cross-peak 5' belongs to CH$_2$ group in accordance with cross-peak sign in the multiplicity-edited ^{13}C-HSQC

Table S5. Chemical shifts of ActS (800 MHz) in D_2O

^1H and ^{13}C chemical shifts and ^1H multiplicities of observed NMR signals of ActS in D_2O observed at 800 MHz NMR. The largest chemical shift difference of ActH and ActS is observed in the 3' group of ribityl moiety (outlined with bold and gray). This evidence argues that ActS is 3' sulfate of ActH.

#	ActS D_2O			Difference with ActH	
	^1H, ppm and multiplicity		^{13}C, ppm	$\Delta\delta$ ^1H, ppm	$\Delta\delta$ ^{13}C, ppm
4			164.26[b]		
5	9.059	s	144.04[a]	0.027	0.26
6	8.053	d 8.8	134.53[a,b]	0.014	0.06
7	7.217	dd 8.8;1.2	117.08[a]	0.009	0.37
9	7.380	d 1.2	101.30[a]	-0.066	-0.30
10a			156.84[b]		-1.08
2'	4.622	m	68.44[a]	0.215	-0.93
3'	**4.551**	**dd 4.0;6.0**	**79.79[a]**	**0.649**	**6.89**
4'	4.189	ddd 6.0;3.0;7.1	70.79[a]	0.239	-1.17
5'H2	3.839	dd 3.0;12.1	62.39[a,c]	-0.013	
5'H3	3.715	dd 7.1;12.1		0.016	0.14

[a] Observed as cross-peak in ^{13}C-HSQC from corresponding directly attached proton

[b] Observed as cross-peak in ^{13}C-HMBC from the singlet proton 5 near 9 ppm

[c] The cross-peak 5' belongs to CH_2 group in accordance with cross-peak sign in the multiplicity-edited ^{13}C-HSQC

Overview of 2D NMR data of ActH and ActS

Figure S4. NMR data interpretation of ActH and ActS from Henlea sp.
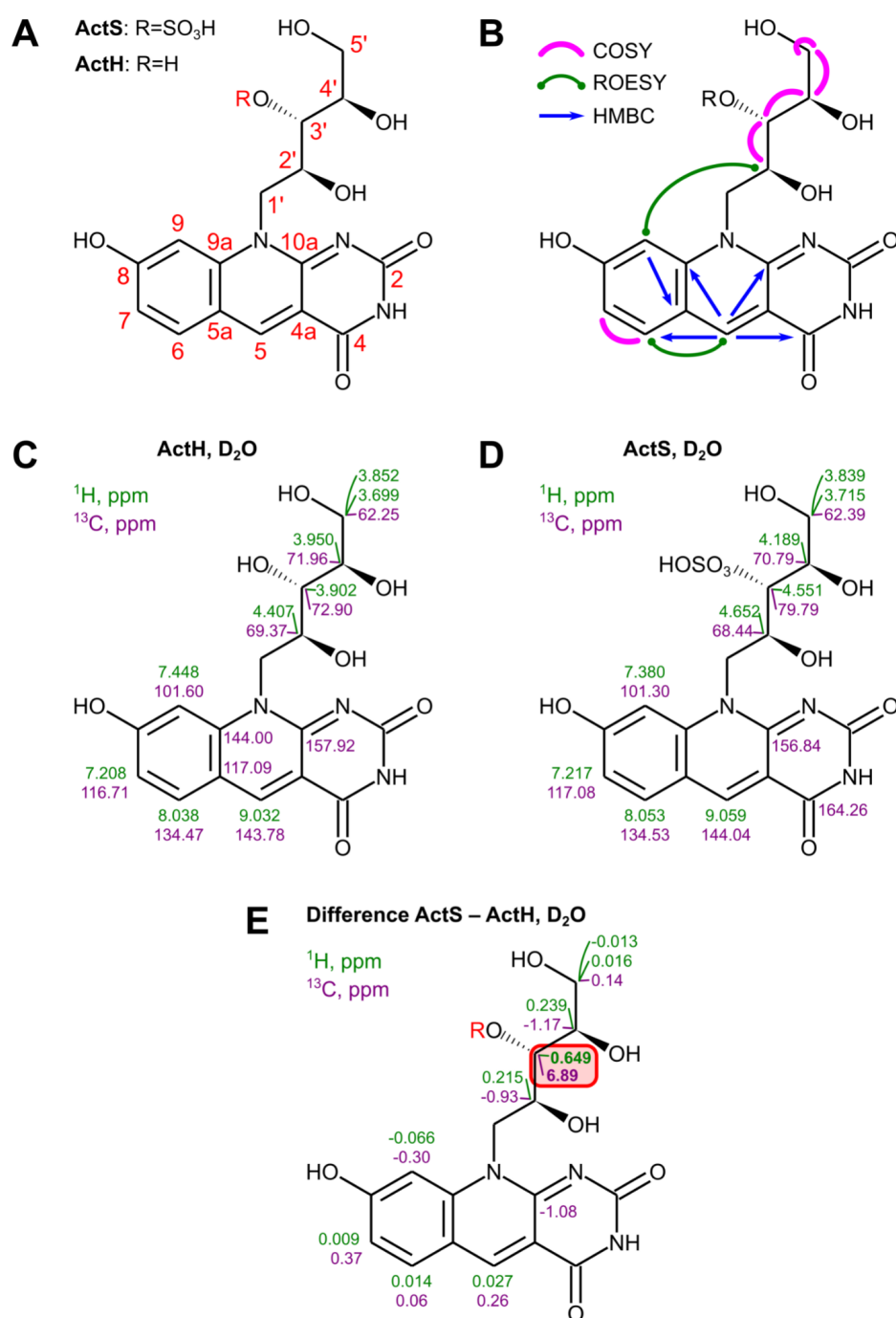
Figure S4. **NMR data interpretation of ActH and ActS from *Henlea sp.*** (**A**) Proposed chemical structures of ActH and ActS with atom numbering matching the Tables S4, S5, S7 and S11. (**B**) Observed cross-peaks in COSY (pink), ROESY (green) and ^{1}H-^{13}C HMBC (blue) 2D NMR spectra of ActH and ActS. These cross peaks were used to assign the chemical shift to the atoms in molecules. (**C**) ^{1}H, ^{13}C chemical shifts of ActH in D_2O at 10°C (see also Table S4. (**D**) ^{1}H, ^{13}C chemical shifts of ActS in the same conditions (D_2O at 10°C, see also Table S5). (**E**) Chemical shift differences of ActH and ActS argue that the sulfate group observed in MS spectra of ActS is located at the 3' hydroxy group of the ribose moiety.

Chemical structure of the ActH and ActS aromatic core

Probe chemical structures (P1-P20) used to pick out the aromatic core of ActH(S)

The 1D and 2D NMR data of ActH(S) aromatic/fluorescent core visualized on figure S5a. The only unambiguous structural element is the 1,2,4-trisubstituted benzene ring, it is probably conjugated to some heterocyclic ring system with either 5-ring cycle (benzofuran or indole, figure S5c) or 6-ring cycle (naphtaline, coumarin or quinoline, figure S5d). We generated 20 probe structures, predicted ^{1}H and ^{13}C chemical shifts with http://nmrdb.org prediction service and visualized (S5b) chemical shift differences on the probe chemical structures.

The best chemical shift match of all eight ^{13}C and four ^{1}H chemical shifts were observed on quinoline structures **(P17-P20)**, figure S5d. Any 5-ring heterocycle could be confidently excluded as incompatible with observed ^{1}H and ^{13}C chemical shifts. Nonetheless, structures **(P17-P20)** do not match the mass spectrometric data, namely brutto formulae should have more carbons, nitrogens and oxygens.

Structure elucidation of ActH(S) aromatic core with LSD software

LSD is an open-source software for Logical Structure Determination (Plainchont et al. 2013; Januar et al. 2016; Nuzillard and Plainchont 2018), it utilizes the NMR data (chemical shifts and 2D correlations) as input and produces ranked chemical structures compatible with NMR data as output. We downloaded the LSD software (Linux distribution) and installed following instructions from the official github webpage https://nuzillard.github.io/PyLSD/INSTALL.html . Program integrity, usability and consistency was verified by running standard examples provided with distribution: input files benzene.lsd, pinene.lsd and strych.lsd resulted in expected output of benzene (1st structure out of 212 possible isomers, see (Plainchont et al. 2013) for details), pinene and strychnine.

For structural resurrection of ActH(S) aromatic core we declared the $C_{11}H_7N_3O_3$ brutto formula (see figure S6). We have ^{1}H/^{13}C chemical shifts of four aromatic CH groups in ^{13}C-HSQC NMR and additionally four ^{13}C chemical shifts of carbons visible in the ^{13}C-HMBC NMR spectra of either ActH or ActS (figure 4 in the main text). Consequently, we have no information about chemical shifts of three carbon atoms of the aromatic core. We explicitly declared 1,2,4-trisubstituted benzene which were identified by characteristic ^{1}H multiplicity patterns. One of 6 benzene carbons was not visible in NMR. We additionally linked CH singlet to the benzene ring because of observed ROESY though-space connectivity. All eleven carbon atoms in the structure were declared in sp2 configuration.

Unfortunately, the LSD software produced enormous output with 3,459,333 structures and failed to sort them. We modified the open-source software and used a computational cluster with 256G RAM and 256G swap to predict all chemical shifts and rank structures. Manual inspection of the LSD output fetched out numerous N-N, N-O and O-O chemical bonds in LSD solutions. That type of chemical bonds are highly improbable in natural products. To resolve the problem we introduced (N/O)-(N/O) ban in the LSD input file (figure S6, magenta rectangle). With that ban LSD generated only 190,469 solutions. We manually explored the first 2,000 structures with the best ^{13}C chemical shifts match Δ (figure S7A). Unfortunately, most LSD structures are non-planar and could not be aromatic and fluorescent. We manually selected several groups (figure S7B, C) of planar and probably fluorescent structures.

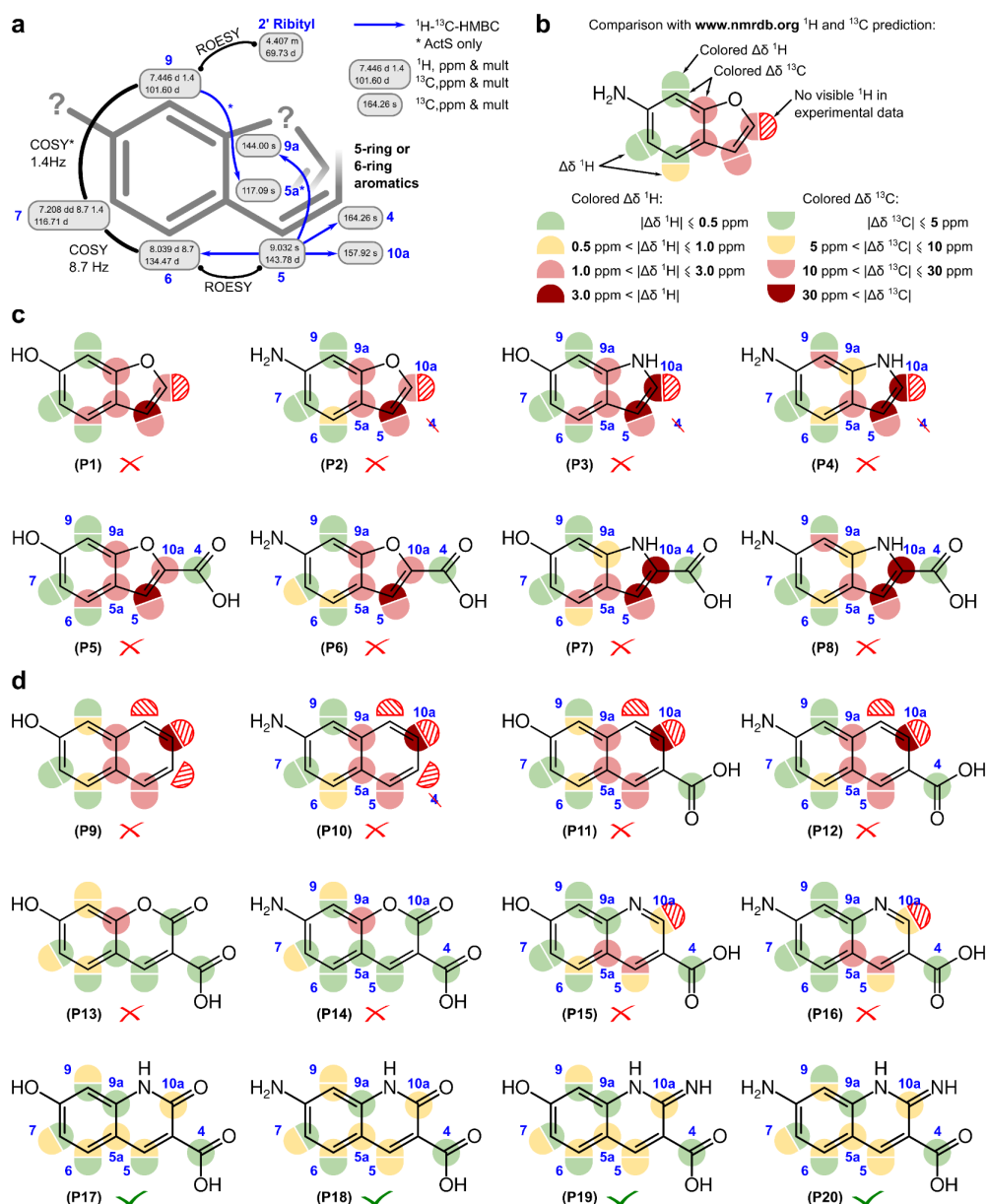# Figure S5. Probe structures used to pick out the aromatic core of ActH(S)

Figure S5. **Probe chemical structures (P1-P20) used to pick out the aromatic core of ActH and ActS. (a)** Summary of NMR data collected for both ActH and ActS, data specific for ActS only is labeled with star. Experimental ^{1}H and ^{13}C chemical shifts of ActH (or ActS*) are in gray ovals. Chemical structure right to the phenol ring is ambiguous: both 5- and 6-ring aromatics should be considered. Atom numbers (in blue) are in accordance with the finally accepted structures of ActH and coincide with other figures and tables in this manuscript. **(b)** Differences of the predicted ^{1}H and ^{13}C chemical shift values (www.nmrdb.org online prediction service) and experimental ones are visualized over probe chemical structures. **(c)** Probe structures with 5-ring benzofuran (P1-P2,P5-P6) and indole (P3-P4, P7-P8) skeletons were rejected because large and systematic chemical shift differences are located in the 5-ring. Discrepancies are most obvious for NMR groups 5, 5a, 9a, 10. Nonetheless, chemical shifts of NMR groups 7 and 9 are in good agreement with the experiment. **(d)** Probe chemical structures with 6-ring (naphtaline P9-P12, coumarine P13-P14 and quinoline P15-P20) structures sequentially improve coincidence with experimental chemical shifts. Last four structures P17-P20 are in good agreement with all available NMR data. See table S6 for predicted chemical shift values and differences with experimental values.

Table S6. Chemical shift differences for probe structures

Experimental ^1H and ^{13}C chemical shifts of the aromatic part of ActH(S), predicted chemical shifts of 20 probe structures **(P1)**-**(P20)** and visualized differences of experimental and predicted chemical shifts.
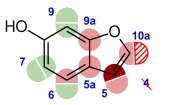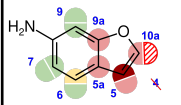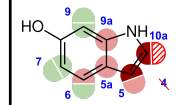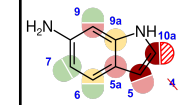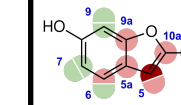
	Experimental chemical shifts		Predicted ^1H and ^{13}C chemical shifts for probe structures, www.nmrdb.org prediction service														
	ActH(S) D2O		(P1)		(P2)		(P3)		(P4)		(P5)		(P6)		(P7)		(P8)	
#	^1H	^{13}C	^1H	^{13}C	^1H	^{13}C	^1H	^{13}C	^1H	^{13}C	^1H	^{13}C	^1H	^{13}C	^1H	^{13}C	^1H	^{13}C
4*		164.26										162.8		162.8		162.5		162.5
5	9.032	143.78	6.578	106.6	6.542	106.6	6.576	102.6	6.548	102.6	7.870	112.8	7.827	112.8	7.019	108.0	6.973	108.0
5a		117.09		127.9		127.9		127.6		127.6		128.3		128.3		128.2		128.2
6	8.039	134.47	7.775	121.1	7.700	127.8	7.799	119.7	7.973	127.8	8.091	121.1	8.048	127.8	7.467	119.7	7.592	127.8
7	7.208	116.71	7.124	115.7	6.762	114.3	6.791	115.7	6.888	114.3	7.211	115.7	6.662	114.3	6.873	115.7	6.765	114.3
9	7.446	101.60	7.192	98.3	7.238	101.4	7.170	101.4	7.092	115.0	7.084	98.3	7.252	101.4	7.144	101.4	7.145	115.0
9a		144.00		155.7		155.1		130.6		136.3		156.7		155.3		136.3		136.3
10a		157.92		145.6		145.6		124.7		124.7		146.2		146.2		127.1		127.1

4* - ^{13}C from ActS

Visualized difference between experimental and predicted chemical shifts for probe structures

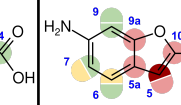| #	P1 ^1H	P1 ^{13}C	P2 ^1H	P2 ^{13}C	P3 ^1H	P3 ^{13}C	P4 ^1H	P4 ^{13}C	P5 ^1H	P5 ^{13}C	P6 ^1H	P6 ^{13}C	P7 ^1H	P7 ^{13}C	P8 ^1H	P8 ^{13}C
4										-1.5		-1.5		-1.8		-1.8
5	-2.454	-37.2	-2.490	-37.2	-2.456	-41.2	-2.484	-41.2	-1.162	-31.0	-1.205	-31.0	-2.013	-35.8	-2.059	-35.8
5a		10.8		10.8		10.5		10.5		11.2		11.2		11.1		11.1
6	-0.264	-13.4	-0.339	-6.7	-0.240	-14.8	-0.066	-6.7	0.052	-13.4	0.009	-6.7	-0.572	-14.8	-0.447	-6.7
7	-0.084	-1.0	-0.446	-2.4	-0.417	-1.0	-0.320	-2.4	0.003	-1.0	-0.546	-2.4	-0.335	-1.0	-0.443	-2.4
9	-0.254	-3.3	-0.208	-0.2	-0.276	-0.2	-0.354	13.4	-0.362	-3.3	-0.194	-0.2	-0.302	-0.2	-0.301	13.4
9a		11.7		11.1		-13.4		-7.7		12.7		11.3		-7.7		-7.7
10a		-12.3		-12.3		-33.2		-33.2		-11.7		-11.7		-30.9		-30.9

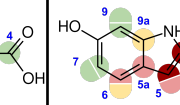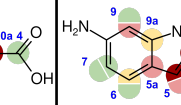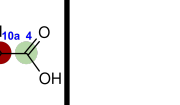|	Experimental chemical shifts		Predicted ¹H and ¹³C chemical shifts for probe structures, www.nmrdb.org prediction service														
	ActH(S) D2O		(P9)		(P10)		(P11)		(P12)		(P13)		(P14)		(P15)		(P16)
#	¹H	¹³C	¹H	¹³C	¹H	¹³C	¹H	¹³C	¹H	¹³C	¹H	¹³C	¹H	¹³C	¹H	¹³C	¹H	¹³C
4*		164.26						167.1		167.1		169.2		169.2		165.5		165.5
5	9.032	143.78	7.786	127.7	7.764	127.7	8.018	127.3	7.929	127.3	8.705	148.5	8.642	148.5	8.378	124.5	8.297	124.5
5a		117.09		130.9		130.9		131.8		131.8		118.2		118.2		128.5		128.5
6	8.039	134.47	7.558	129.4	7.434	128.9	7.919	129.4	7.725	128.9	8.136	127.6	7.932	131.1	8.138	125.7	8.343	129.5
7	7.208	116.71	6.978	117.8	7.196	118.1	6.983	117.8	6.950	118.1	6.515	115.7	6.628	114.3	7.077	117.8	7.042	118.1
9	7.446	101.60	7.352	108.8	7.600	102.7	7.419	108.8	7.838	102.7	6.626	95.8	6.720	99.2	7.678	104.4	7.665	98.6
9a		144.00		131.4		132.7		131.4		132.7		155.4		157.1		147.3		147.0
10a		157.92		126.4		126.4		125.0		125.0		155.9		155.9		149.2		149.2

4* - ¹³C from ActS	Visualized difference between predicted and experimental chemical shifts for probe structures

#	(P9) ¹H	(P9) ¹³C	(P10) ¹H	(P10) ¹³C	(P11) ¹H	(P11) ¹³C	(P12) ¹H	(P12) ¹³C	(P13) ¹H	(P13) ¹³C	(P14) ¹H	(P14) ¹³C	(P15) ¹H	(P15) ¹³C	(P16) ¹H	(P16) ¹³C
4						2.8		2.8		5.0		5.0		1.2		1.2
5	-1.246	-16.1	-1.268	-16.1	-1.014	-16.5	-1.103	-16.5	-0.327	4.7	-0.390	4.7	-0.654	-19.3	-0.735	-19.3
5a		13.8		13.8		14.7		14.7		1.1		1.1		11.4		11.4
6	-0.481	-5.1	-0.605	-5.6	-0.120	-5.1	-0.314	-5.6	0.097	-6.9	-0.107	-3.4	0.099	-8.8	0.304	-5.0
7	-0.230	1.1	-0.012	1.4	-0.225	1.1	-0.258	1.4	-0.693	-1.0	-0.580	-2.4	-0.131	1.1	-0.166	1.4
9	-0.094	7.2	0.154	1.1	-0.027	7.2	0.392	1.1	-0.820	-5.8	-0.726	-2.4	0.232	2.8	0.219	-3.0
9a		-12.6		-11.3		-12.6		-11.3		11.4		13.1		3.3		3.0
10a		-31.5		-31.5		-32.9		-32.9		-2.0		-2.0		-8.7		-8.7

Table S6 (finished)

	Experimental chemical shifts		Predicted ^{1}H and ^{13}C chemical shifts for probe structures, www.nmrdb.org prediction service							
	ActH(S) D2O		(P17)		(P18)		(P19)		(P20)	
#	^{1}H	^{13}C	^{1}H	^{13}C	^{1}H	^{13}C	^{1}H	^{13}C	^{1}H	^{13}C
4*		164.26		164.6		164.6		164.5		163.5
5	9.032	143.78	8.554	136.9	8.487	136.9	8.099	136.9	8.058	136.9
5a		117.09		123.0		123.0		123.0		123.0
6	8.039	134.47	7.917	127.8	7.746	127.0	8.093	127.8	7.678	127.0
7	7.208	116.71	6.345	115.7	6.537	114.3	6.639	115.7	6.479	114.3
9	7.446	101.60	6.702	96.7	6.576	95.7	6.536	96.7	7.109	95.7
9a		144.00		140.2		140.2		140.2		140.2
10a		157.92		163.2		163.2		150.9		150.9

4* - ^{13}C from ActS	Visualized difference between predicted and experimental chemical shifts for probe structures			
4		0.3		0.3		0.2		-0.8
5	-0.478	-6.9	-0.545	-6.9	-0.933	-6.9	-0.974	-6.9
5a		5.9		5.9		5.9		5.9
6	-0.122	-6.7	-0.293	-7.4	0.054	-6.7	-0.361	-7.4
7	-0.863	-1.0	-0.671	-2.4	-0.569	-1.0	-0.729	-2.4
9	-0.744	-4.9	-0.870	-5.9	-0.910	-4.9	-0.337	-5.9
9a		-3.8		-3.8		-3.8		-3.8
10a		5.3		5.3		-7.0		-7.0

Figure S6. Input file for the LSD software

```
; Input file for LSD for structure elucidation of
; the aromatics part of ActH(S) cofactor from
; Henlea sp // Maxim A. Dubinnyi


FORM "C 11 H 7 N 3 O 3"
PIEC 1


; Benzene ring 1-6 starts

; 1 - Aromatic large doublet in 1H
MULT 1 C 2 1
SHIX 1 134.47
HSQC 1 1
SHIH 1 8.039 ; large d(8.7Hz)
HMBC 1 7


; 2 - Aromatic doublet of doublets in 1H
MULT 2 C 2 1
SHIX 2 116.71
HSQC 2 2
SHIH 2 7.208 ; dd(8.7Hz,1.4Hz)


; 3 - Carbon in benzene ring,
; invisible in HSQC/HMBC
; probably N- or O- substituted
; located between dd and small d
MULT 3  C 2 0


; 4 - Aromatic small doublet in 1H
MULT 4 C 2 1
SHIX 4 101.60
HSQC 4 4
SHIH 4 7.446


; Carbons 5 and 6 are visible in 13C-HMBC only
MULT 5 C 2 0
SHIX 5 144.00
HMBC 5 7


MULT 6 C 2 0
SHIX 6 117.09
HMBC 6 4
; Benzene ring 1-6 finished


; Aromatic singlet in 1H
MULT 7 C 2 1
SHIX 7 143.78
HSQC 7 7
SHIH 7 9.032


; Explicitly define aromatic benzene ring
BOND 1 2 ; supported by COSY, J=8.7 Hz
BOND 2 3
BOND 3 4
BOND 4 5
```

```
BOND 5 6
BOND 6 1


; Carbone C7/H7 (singlet) have ROE with C1/H1,
; add bond to the ring
BOND 6 7


; Carbons C8 and C9 are observed in 13C-HMBC
MULT 8 C 2 0
SHIX 8 157.92
HMBC 8 7


MULT 9 C 2 0
SHIX 9 164.26
HMBC 9 7


; Carbons C10 and C11 are invisible in NMR
; They are assumed to be in sp2 configuration
; and have no directly attached protons
; No additional protons were observed in 1H NMR
MULT 10  C 2 0
MULT 11 C 2 0



; Explicitly state Oxygens (O) and Nitrogens (N)
; atoms, no NMR information,
; Either sp2 or sp3 (2 3)
; With 0 to 2 protons attached O:(0 1) N:(0 1 2)
MULT 12 O (2 3) (0 1)
MULT 13 O (2 3) (0 1)
MULT 14 O (2 3) (0 1)
MULT 15 N (2 3) (0 1 2)
MULT 16 N (2 3) (0 1 2)
MULT 17 N (2 3) (0 1 2)
```

```
; BAN for N-N, N-O and O-O bonds
; LIST L1 is the list of all N/O atoms
LIST L1 12 13 14 15 16 17
; LIST L2 is the list of all carbons
LIST L2 1 2 3 4 5 6 7 8 9 10 11
; do ban for N/O-N/O bonds:
; All (0) neighbors of L1 (N/O) should be L2 (C)
PROP L1 0 L2
```

```
; ALLOW duplicate structures to be generated by LSD
; in our tests (not shown) default behavior drops
; some solutions
; DUPL P1
; P1=0: duplicate structures may be produced.
; P1=1: duplicate solutions are removed.
; P1=2: duplicate structures are removed (default).
DUPL 0


EXIT
```

Figure S6. **Input file for the LSD software.** It was executed in two versions: (A) without a magenta block that bans (N/O)-(N/O) bonds in chemical structures proposed. That version resulted in 3,459,333 solutions that we were not able to explore. The second run (B) with a magenta (N/O)-(N/O) ban block resulted in 190,469 solutions, and we explored the first 2,000 (best 2,000) solutions manually (see figure S7).
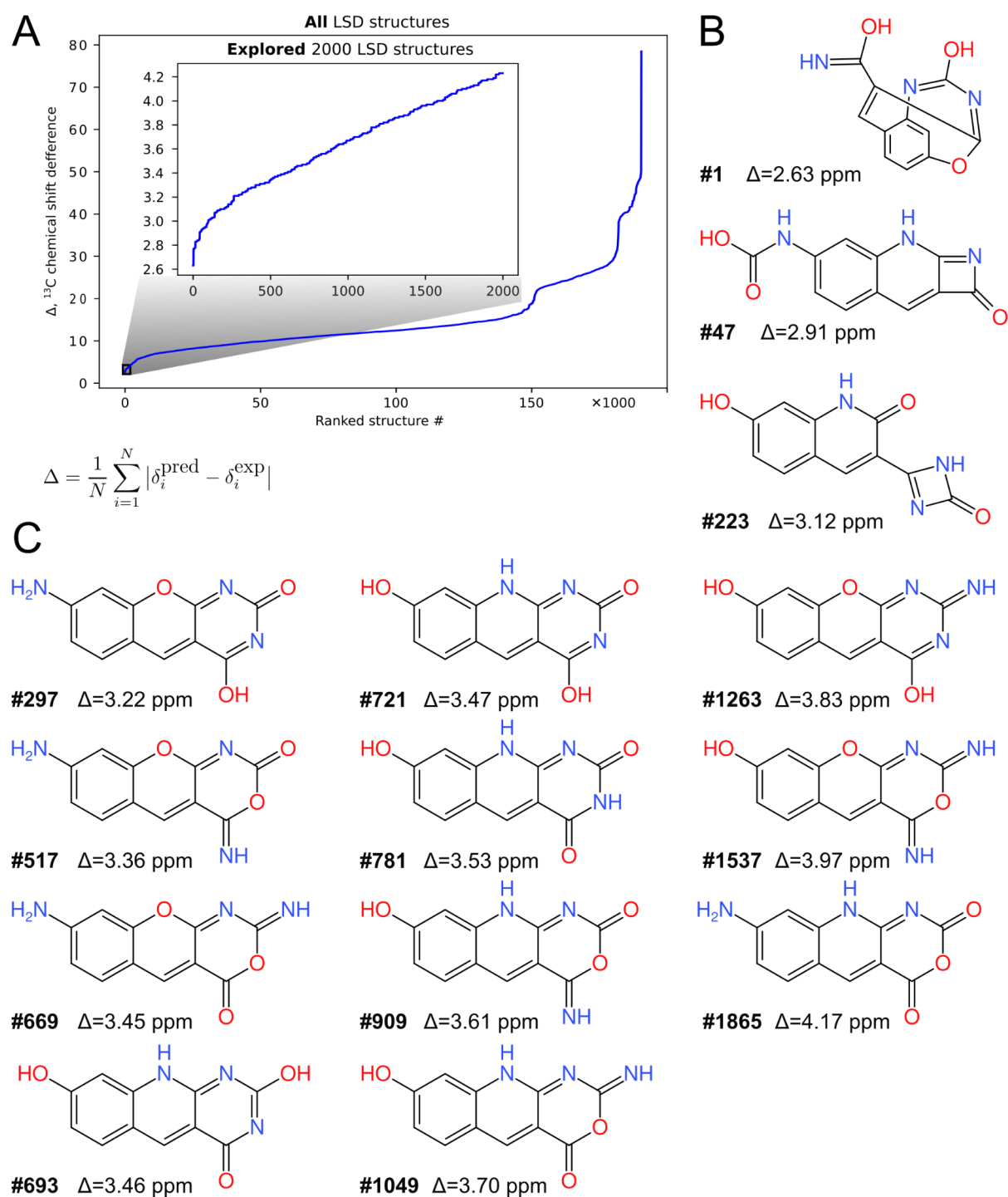
Figure S7. Selected output of the LSD software

Figure S7. **Selected of the LSD software. (A)** Plot of mean ^{13}C chemical shift differences Δ of 190,469 ranked LSD structures. Inset: Δ of the first 2,000 manually explored structures. **(B)** Selected LSD structures. The first structure **#1** have bond connectivities incompatible with expected fluorescence of ActH(S), the same is true for the predominant number of LSD structures. Structures **#47** and **#223** are the first planar solutions found. **(C)** The series of planar (probably fluorescent) structures with N/O atoms interchanged and tautomeric forms picked out. All those structural differences have a little effect on predicted NMR chemical shifts and mean ^{13}C chemical shift difference Δ. These structures could be accepted as compatible with 1D and 2D NMR data collected in the present work.

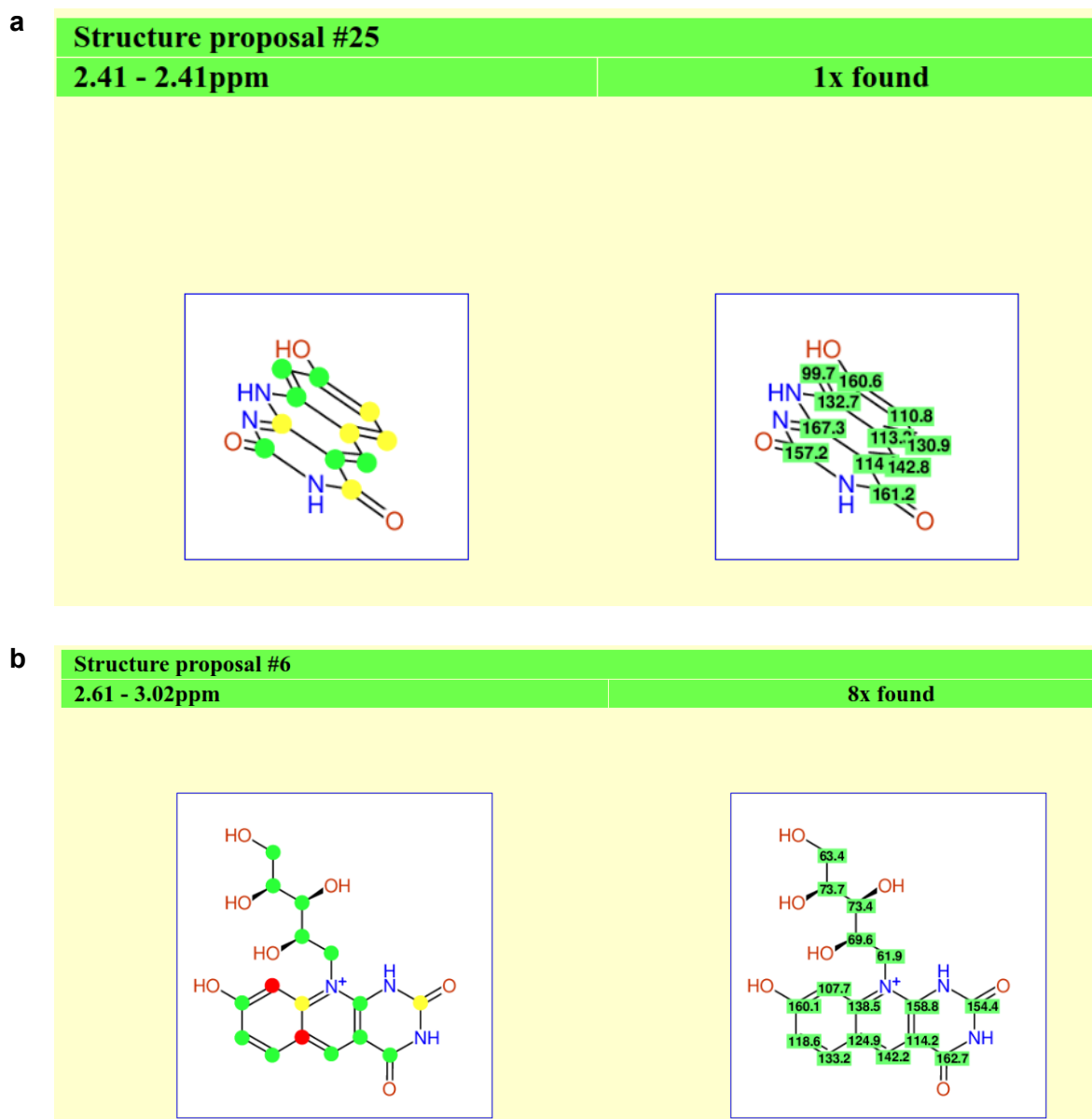# Figure S8. Selected CSEARCH output compatible with 2D NMR of ActH(S)

a

b

Figure S8. **Selected CSEARCH output manually verified for compatibility with 2D NMR.** **(A)** Selected hit #25 from the first ^{13}C "Spectral similarity search" query, it includes ^{13}C NMR of the ActH aromatic core and molecular weight 229 Da. The search resulted in brutto formulae $C_{11}H_7N_3O_3$ consistent with the MSn data. **(B)** Manually selected hit #6 from a query with ^{13}C ActH data, molecular weight 363 Da resulted in brutto formulae $C_{16}H_{17}N_3O_7$ as expected from the MSn data, note the presence of ribitol fragment and the same aromatic core as found in **(A)**. The structure **(B)** is the finally accepted chemical structure of ActH.

Table S7. NMR data of ActH in comparison with (Kuo et al. 1989)

Table S7. Comparison of NMR chemical shifts reported in (Kuo et al. 1989) with chemical shifts of the *Henlea sp.* activator ActH in the same solvent MeOD (Table S4 above). We impute the observed discrepancies to different acidity of MeOD in (Kuo et al. 1989) and in the sample isolated from the *Henlea sp.* in this work.

#	^{1}H, ppm and multiplicity		^{13}C, ppm	Δδ ^{1}H, ppm	Δδ ^{13}C, ppm
2			162.5		
4			158.1		
4a			114.5		
5	8.56		140.1	-0.40	**-2.19**
5a			108.0		
6	7.65	d (J=8)	133.4	-0.35	-0.30
7	6.95	d (J=3)[a]	117.6	-0.17	1.40
8			158.5		
9	6.74	dd (J=8, 3)[b]	102.1	**-0.80**	0.31
9a			144.3		
10a			156.7		
1'a	5.04		47.7		
1'b	4.67				
2'	4.35	ddd (J=9, 7, 4)	69.8	-0.09	-0.55
3'	3.75	dd (J=7, 5)	73.8	-0.06	-0.12
4'	3.86		72.6	-0.03	-0.15
5'a	3.83		63.2	-0.05	-0.20
5'b	3.66			-0.04	
Chemical shift r.m.s.d., ppm				**0.26**	**0.99**

[a] Incorrect multiplicity reported, probably it should be dd(J=3, 8)
[b] Incorrect multiplicity reported, probably it should be d(J=3)

Total synthesis of ActH

Table S8. 3-((t-butyldiphenyl)oxy)anilin (1):

1
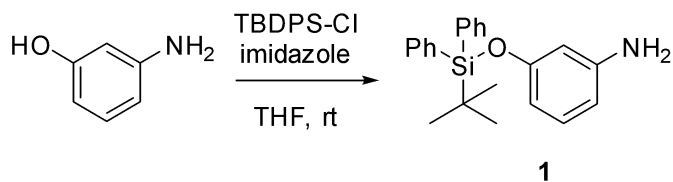
Imidazole (2.50 g, 36.65 mmol) and 3-aminophenol (2.00 g, 18.33 mmol) were dissolved in absolute THF. The mixture was stirred at ambient temperature for 30 minutes. Then diphenyl-*t*-butylchlorosilane (7.56 g, 27.49 mmol) was added by drops. The white precipitate was observed. The resulting suspension was stirred overnight. After full conversion (detected by TLC: SiO$_2$, chloroform/ethanol 9:1, R$_f$ 0.8) 100 mL of water were added and the product was extracted by ether (4x100 mL). The product as a yellow oil **1** was purified by column chromatography (Hex/EtOAc=70:30) with yield 5.50 g (86%).

^{1}H and ^{13}C NMR (700 MHz and 176 MHz, CDCl$_3$, 30°C) see table below. Assignment was verified by 2D NMR: ^{13}C-HSQC, ^{13}C-HMBC, ^{15}N-HMBC, DQF-COSY, ^{13}C-HSQC-TOCSY. Protons H2 and H4 were discriminated by ^{15}N-HMBC contact to the NH$_2$ group (contact observed for H2 but not for H4).

Table S8. ^{1}H, ^{13}C and ^{15}N chemical shift assignment of **1**.

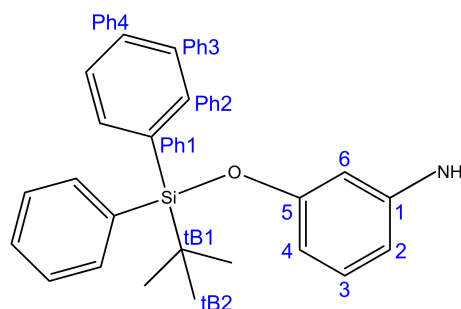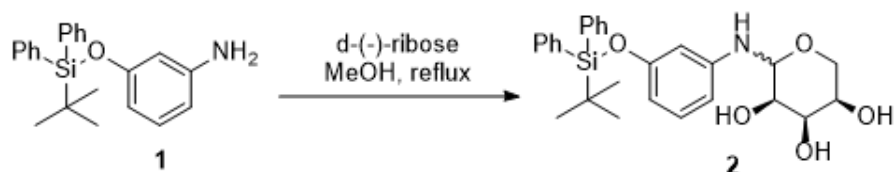| Atom	^{1}H, ppm	^{1}H mult, Hz	nH	^{13}C, ppm
1	—	—		147.53
2	6.290	ddd (J = 8.0, 2.2, 0.9)	1H	108.35
3	6.933	t (J = 8.0)	1H	129.79
4	6.256	ddd (J = 8.0, 2.2, 0.9)	1H	110.34
5	—	—		156.69
6	6.24	t (J = 2.2)	1H	106.83
NH$_2$	n.o.	n.o.		55.01(^{15}N)
Ph1	—	—		133.29
Ph2	7.815	dd (J = 8.2, 1.3)	4H	135.59
Ph3	7.449	t (J = 7.5)	4H	127.77
Ph4	7.500	tt (J = 7.5, 1.3)	2H	129.86
tB1	—	—		19.53
tB2	1.179	s	9H	26.61

Table S9. 2-((3-((t-butildiphenylsilyl)oxy)phenyl)amino)tetrahydro-2H-pirane-3, 4,5-triol (2):

D-(-)-ribose (1.24 g, 8.17 mmol) and **1** (2.66 g, 7.57 mmol) were dissolved in 26 mL of MeOH. The reaction mixture was stirred at reflux until full conversion (detected by TLC: SiO_2, chloroform/ethanol 9:1, R_f 0.25) under inert atmosphere. After that the solvent was distilled under reduced pressure and the residue was redissolved in 26 mL of methylene chloride. The solution was washed with brine (5x20 mL) and dried over sodium sulfate. Then the solvent was distilled under reduced pressure and the product **2** 2,42 g (67%) was observed as a white sticky solid and used in the next step without further purification..

Chemical structure of **2** was verified by 1D (^{1}H and ^{13}C) and 2D NMR (^{13}C-HSQC, ^{15}N-HSQC, ^{13}C-CT-HMBC, 2D DQF-COSY, 2D TOCSY (200ms), ^{13}C-HSQC-TOCSY 200ms) in CDCl$_3$, 700 MHz at 30°C. Ribose was found to be in hexose conformation (because of H5'→C1' and H1'→C5 HMBC contacts), two forms were observed in NMR at 3.6:1 ratio. The conformational heterogeneity was because of non-selectivity in the new NH-C1' bond. For NMR assignment (700MHz, CDCl$_3$, 30°C) see figure and table below.
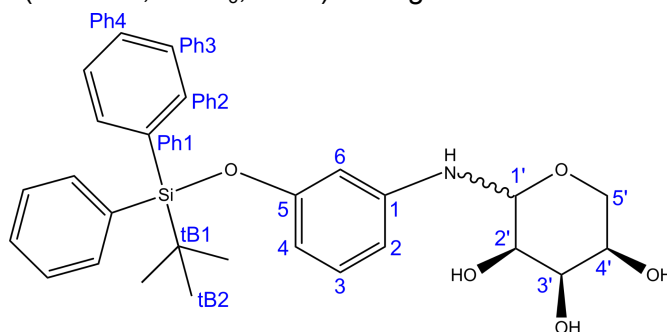

Table S9. ^{1}H, ^{13}C and ^{15}N chemical shift assignment of the observed forms of **2**.

Atom	Form 1 (integral of ^{1}H = 3.6)				Form 2 (integral of ^{1}H = 1.0)			
	^{1}H, ppm	^{1}H mult, Hz	nH	^{13}C, ppm	^{1}H, ppm	^{1}H mult, Hz		^{13}C, ppm
1	—	—		145.79	—	—		146.43
2	6.313	dd (J = 8.1, 2.1)	1H	107.63	6.378	dd (J = 8.1, 2.1)	1H	108.15
3	6.972	t (J = 8.1)	1H	129.83	6.974	t (J = 8.1)	1H	129.86
4	6.327	dd (J = 8.1, 2.1)	1H	111.04	6.343	dd (J = 8.1, 2.1)	1H	111.85
5	—	—		156.73	—	—		156.70
6	6.244	t (J = 2.1)	1H	105.64	6.328	overlap	1H	106.74
NH	5.158	Broad (~90 Hz)		78.88 (^{15}N)	5.297	Broad (~90 Hz)		n.o.
1'	4.375	Broad (~3 Hz)	1H	82.54	4.712	d (J = 7.8)	1H	82.34
2'	3.862	m	1H	71.68	3.471	dd (J = 11.2, 4.9)	1H	71.08
3'	3.598	t (J = 3.3)	1H	69.59	4.199	t (J = 3.0)	1H	69.58

Atom	^{1}H, ppm	^{1}H mult, Hz	nH	^{13}C, ppm	^{1}H, ppm	^{1}H mult, Hz	nH	^{13}C, ppm
4'	3.849	m	1H	68.81	3.818	dd (J = 12.0, 3.5)	1H	67.55
5'	3.911	dd (J = 2.5, 12.8)	1H	66.69	3.738	dd (J = 4.7, 11.2)	1H	64.17
	3.312	dd (J = 1.2, 12.8)	1H		3.546	dd (J = 9.6, 11.2)	1H	
Ph1	—	—		133.23	—	—		133.23
Ph2	7.795	m	4H	135.59	7.795	m	4H	135.59
Ph3	7.421	t (J = 7.5)	4H	127.77	7.421	t (J = 7.5)	4H	127.77
Ph4	7.469	t (J = 7.5)	2H	129.85	7.469	t (J = 7.5)	2H	129.85
tB1	—	—		19.57	—	—		19.57
tB2	1.159	s	9H	26.61	1.165	s	9H	26.62

Table S10. 2-((3-((t-butildiphenylsilyl)oxy)phenyl)amino)pentane-1,2,3,4-tetraol (3):
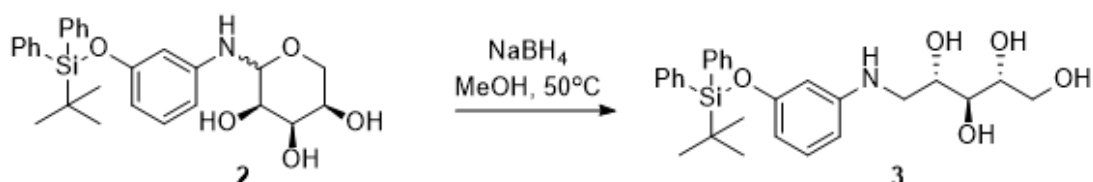
Sodium borohydride (1.53 g, 39.96 mmol) was added portionwise to a cooled (0°C) solution of **2** (2.42 g, 4.99 mmol) in 26 mL of dry methanol. After addition the reaction mixture was heated to 50°C and stirred under an inert atmosphere for 16 h. After full conversion (detected by TLC: SiO$_2$, chloroform/ethanol 9:1, R$_f$ 0.2) the mixture was quenched with saturated NH$_4$Cl (150 mL) and extracted with methylene chloride (5x50 mL). The organic layers were combined and dried over sodium sulfate. The solvent was distilled under reduced pressure and the product was purified by column chromatography (SiO$_2$, chloroform/ethanol 9:1). The product was observed as a white sticky solid (1.07 g, 44%).

Chemical structure of **3** was verified by ^{1}H, 2D ^{13}C-HSQC and 2D DQF-COSY NMR (700MHz, CDCl$_3$, 30°C). Fast degradation was observed overnight in ^{1}H NMR at those conditions, compound **3** was stored frozen and used immediately for the next stage.
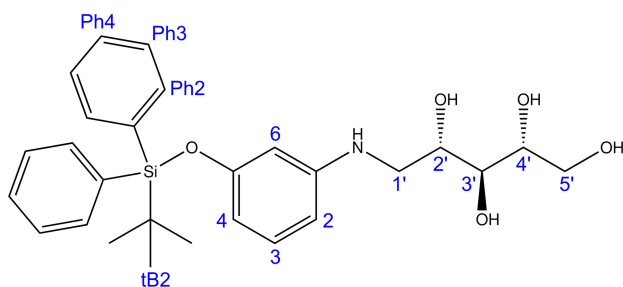
Table S10. ^{1}H and ^{13}C chemical shift assignment of **3**.

Atom	^{1}H, ppm	^{1}H mult, Hz	nH	^{13}C, ppm
2	6.358	ddd (J = 8.3, 2.2, 0.6)	1H	108.39
3	7.072	t (J = 8.3)	1H	129.63

4	6.436	ddd (J = 9.0, 2.2, 0.6)	1H	110.29
6	6.178	t (J = 2.3)	1H	107.11
1'	3.429	dd (J = 8.9, 6.3)	1H	49.78
	3.359	dd (J = 8.9, 7.0)	1H	
2'	4.294	q (J = 6.7)	1H	74.49
3'	3.794	t (J = 6.7)	1H	73.30
4'	3.835	dt (J = 6.2, 4.0)	1H	72.34
5'	3.900	d (J = 4.0)	2H	63.58
Ph2	7.803	ddd (J = 8.0, 2.3, 1.3)	4H	135.60
Ph3	7.435	ddd (J = 7.9, 2.2, 0.9)	4H	127.82
Ph4	7.484	m	2H	129.88
tB2	1.177	s	9H	26.60

8-hydroxy-10-(2,3,4,5-tetrahydroxypentyl)pyrimido[4,5-b]-quinoline-2,4(3H, 10H)dion (4):

3
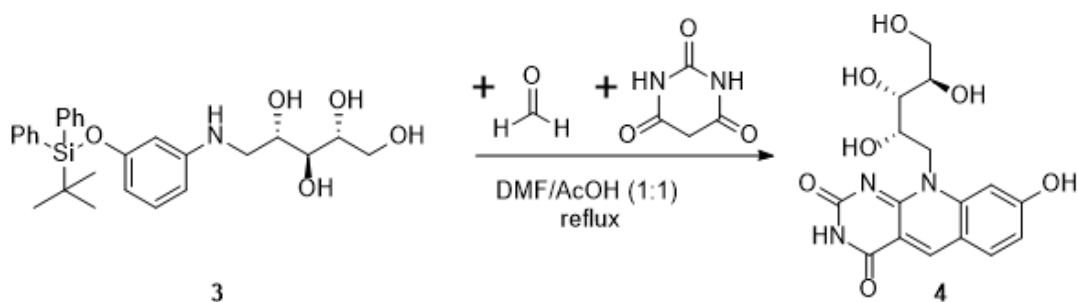
Paraformaldehyde (0.006 g, 0.21 mmol), barbituric acid (0.03 g, 0,21 mmol) and **3** (0.1 g, 0.21 mmol) were dissolved in 2 mL of mixture of DMF and acetic acid (1:1). The mixture was heated to 120ºC and stirred for 30 minutes under an inert atmosphere. The conversion was detected by TLC (SiO$_2$, chloroform/ethanol 7:3, R$_f$ 0.4). After full conversion has been reached the acetic acid was distilled under reduced pressure. Then 10 mL of ether were added to receive yellow precipitate. The precipitate was filtered and purified by reversed-phase chromatography (MeCN/H$_2$O 5 => 50). The product was observed as a dark-yellow powder (0.2 g, 31%).

NMR assignment in MeOD: see the next section.

Comparison of natural and synthetic ActH

Table S11. Chemical shifts of natural and synthetic ActH

Table S11. [1]H and ^{13}C chemical shifts and ^{1}H multiplicities of synthetic ActH at the same conditions as ActH from *Henlea sp.* (MeOD, 10°C, acidic pH 3.31, 700 MHz for synthetic ActH and 800 MHz for natural AtcH). The chemical shift differences with literature data (Kuo et al. 1989) is in line with pH-dependence of NMR spectra. The complete match of the observed chemical shifts with ActH from *Henlea sp.* proofs that *Henlea* activator ActH is the same substance as archeal cofactor F0.

#	ActH synthetic in MeOD			Difference with (Kuo et al. 1989), MeOD		Difference with ActH *Henlea sp.*, MeOD	
	[1]H, ppm and multiplicity		[13]C, ppm	Δδ ^{1}H, ppm	Δδ ^{13}C, ppm	Δδ ^{1}H, ppm	Δδ ^{13}C, ppm
2			n.o				
4			163.21		5.1		
4a			n.o				
5	8.968		142.51	0.41	2.4	0.004	**0.22**
5a			116.40		8.4		
6	7.995	d (J=8.8)	133.77	0.35	0.4	0.000	0.07
7	7.117	dd (J=8.8, 2.1)	116.12	0.17	-1.5	-0.001	-0.08
8			165.48		**7.0**		
9	7.543	d (J=2.1)	101.83	**0.80**	-0.3	0.003	0.04
9a			144.54		0.2		
10a			158.22		1.5		
1'a	4.941		47.97	-0.10	0.3		
1'b	4.589			-0.08			
2'	4.438	m	70.29	0.09	0.5	-0.001	-0.06
3'	3.803	dd (J=7.4, 4.7)	73.83	0.05	0.0	-0.002	-0.09
4'	3.893	m	72.71	0.03	0.1	0.002	-0.04
5'a	3.870	dd (J=3.2, 11.2)	63.30	0.04	0.1	**-0.006**	-0.10
5'b	3.706	dd(J=6.3, 11.2)		0.05		0.002	
Chemical shift r.m.s.d., ppm				**0.26**	**2.97**	**0.003**	**0.11**

Figure S9. Chemical shifts of natural and synthetic ActH on the structure

A Natural ActH from *Henlea sp.*, MeOD

B Synthetic F0, MeOD

C Difference: natural ActH - synthetic F0
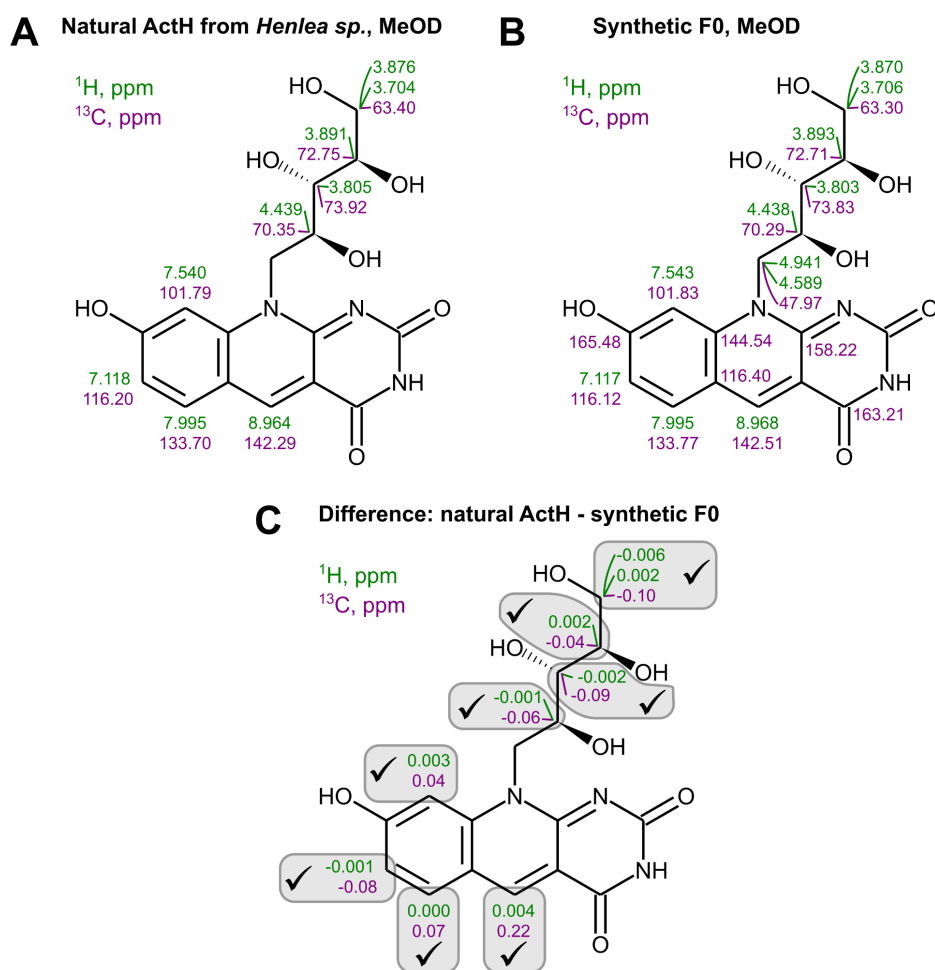
Figure S9. **Bioluminescence activator ActH from *Henlea sp.* is the archeal cofactor F0.** (**A**) Proposed chemical structure and observed ^{1}H,^{13}C chemical shifts of ActH from *Henlea sp.* in acidic MeOD at 10℃. (**B**) Observed ^{1}H,^{13}C chemical shifts of synthetic ActH at the same conditions. (**C**) The complete match of the observed chemical shifts provide unambiguous evidence that ActH from *Henlea sp.* is the archeal cofactor F0.

BL activation by synthetic cofactor F0

Table S12. Activation factor X against concentration of synthetic ActH

Table S12. The BL activation factor X of *Henlea sp.* bioluminescence against concentration of synthetic ActH.

[ActH], μM	Factor X
0,0345	5,4
0,069	7,7
0,115	10,8
0,23	16,8
0,46	22,0
0,92	25,8
2,3	30,5
4,6	32,0

The data were analyzed with Michaelis-Menten kinetics model (Oestreicher and Pinto 1983):

$$X = X_{\max}\frac{S}{S+K_m}$$

Where S is the concentration of the synthetic cofactor F0 added to the reaction. As the result, the best fit values of the Michaelis-Menten parameters were estimated:
$X_{\max} = 33.3 \pm 0.5$ and $K_m = 0.23 \pm 0.01 \mu M$.

Correction of the Michaelis-Menten kinetics for a background bioluminescence

The data presented in table S12 picks the ratio of bioluminescence intensity after and before BL activation by the synthetic bacterial cofactor F0 (X-ratio). The absolute value of BL intensity is extremely hard to reproduce because of sophisticated luciferin (LN) thermal activation procedure: the LN is heated to 100°C for one minute and then cooled to room temperature for one minute. The extent of LN activation reduced rapidly during two minutes. That procedure introduces large variation in the absolute BL intensity due to different factors of LN thermal activation from point to point (data not shown). Nevertheless, X-factor shows an accurate and reproducible Michaelis-Menten curve (Figure 7 in the main text).

The background bioluminescence is presented because some small concentration of ActH and/or ActS is persistent in the luciferase cold extract aliquotes used to start BL reaction. The parameters K_m and $X_{\max}$ determined in the previous section should be corrected for the presence of background bioluminescence due to that persistent activators. The algebraic transformation below illustrates how that correction should be done.

The first, from the definition of the activation factor and Michaelis-Menten equation for the BL activation factor X we have:

$$X = \frac{I - I_0}{I_0} = X_{\max}\frac{S}{S + K_m}$$

The second, straightforward algebraic transformations goes to:

$$I - I_0 = I_0 X_{\max}\frac{S}{S + K_m}$$

$$I = I_0 X_{\max} \frac{S}{S + K_m} + I_0$$

$$I = I_0 X_{\max} \left(\frac{S}{S + K_m} + \frac{1}{X_{\max}} \right)$$

$$I = I_0 X_{\max} \frac{S X_{\max} + S + K_m}{X_{\max}(S + K_m)}$$

$$I = I_0 \frac{(1 + X_{\max})S + K_m}{S + K_m}$$

$$I = I_0(1 + X_{\max}) \frac{(1 + X_{\max})S + K_m}{(1 + X_{\max})(S + K_m)}$$

$$I = I_0(1 + X_{\max}) \frac{(1 + X_{\max})S + K_m}{(1 + X_{\max})S + K_m + X_{\max}K_m}$$

$$I = I_0(1 + X_{\max}) \frac{S + \frac{K_m}{1 + X_{\max}}}{S + \frac{K_m}{1 + X_{\max}} + \frac{X_{\max}}{1 + X_{\max}} K_m}$$

Lets replace the parameters S, K_m and $X_{\max}$ with the new ones $\tilde{S}$, $\tilde{K}_m$ and $\tilde{I}_{\max}$ by the following definitions:

$$\tilde{S} = S + S_0$$

$$S_0 = \frac{K_m}{1 + X_{\max}}$$

$$\tilde{K}_m = \frac{X_{\max}}{1 + X_{\max}} K_m$$

$$\tilde{I}_{\max} = I_0(1 + X_{\max})$$

Then we have the new Michaelis-Menten equation that describes the relation on new parameters:

$$I = \tilde{I}_{\max} \frac{\tilde{S}}{\tilde{S} + \tilde{K}_m}$$

Finally, from the parameters and equation above we extract the estimation S_0 of the background concentration of ActH/ActS:

$$S_0 = \frac{0.23 \mu M}{1 + 33.3} = 0.0067 \mu M$$

and the corrected value of Michaelis-Menten constant

$$\tilde{K}_m = \frac{33.3}{1 + 33.3} 0.23 \mu M = 0.22 \mu M$$

The algebraic transformations above could be made backward providing the proof that the activation factor X follows the Michaelis-Menten kinetics if the bioluminescence itself follows it.

References

DiMarco AA, Bobik TA, Wolfe RS (1990) Unusual coenzymes of methanogenesis. Annu Rev Biochem 59:355–394. https://doi.org/10.1146/annurev.bi.59.070190.002035

Gottlieb HE, Kotlyar V, Nudelman A (1997) NMR Chemical Shifts of Common Laboratory Solvents as Trace Impurities. J Org Chem 62:7512–7515. https://doi.org/10.1021/jo971176v

Januar HI, Zamani NP, Soedharma D, Chasanah E (2016) Logic Structure Determination (LSD) as a Computer Assisted Structure Elucidation (CASE) for Molecular Structure Determination of Cytotoxic Cembranoids from Soft Coral. Squalen Bull Mar Fish Postharvest Biotechnol 11:1–6. https://doi.org/10.15578/squalen.v11i1.177

Kuo MS, Yurek DA, Coats JH, Li GP (1989) Isolation and identification of 7,8-didemethyl-8-hydroxy-5-deazariboflavin, an unusual cosynthetic factor in streptomycetes, from Streptomyces lincolnensis. J Antibiot (Tokyo) 42:475–478. https://doi.org/10.7164/antibiotics.42.475

Nuzillard J-M, Plainchont B (2018) Tutorial for the structure elucidation of small molecules by means of the LSD software. Magn Reson Chem 56:458–468. https://doi.org/10.1002/mrc.4612

Oestreicher EG, Pinto GF (1983) Pocket computer program for fitting the Michaelis-Menten equation. Comput Biol Med 13:309–315. https://doi.org/10.1016/0010-4825(83)90008-2

Petushkov VN, Rodionova NS (2018) Low-Molecular-Weight Components of Luminescent Reaction of the Siberian Enchytraeid Henlea sp. Dokl Biochem Biophys 481:212–216. https://doi.org/10.1134/S1607672918040099

Plainchont B, de Paulo Emerenciano V, Nuzillard J-M (2013) Recent advances in the structure elucidation of small organic molecules by the LSD software. Magn Reson Chem 51:447–453. https://doi.org/10.1002/mrc.3965